Simplifying Nanowire Hall Effect Characterization by Using a Three-Probe Device Design

Hultin, Olof; Otnes, Gaute; Samuelson, Lars; Storm, Kristian

Published in:
Nano Letters

DOI:
10.1021/acs.nanolett.6b04723

2017

Document Version:
Peer reviewed version (aka post-print)

Simplifying Nanowire Hall Effect Characterization by Using a Three-Probe Device Design

Olof Hultin[1], Gaute Otnes[1], Lars Samuelson[1] and Kristian Storm[2]*

1. Division of Solid State Physics, Lund University, P.O. Box 118, SE-221 00 Lund, Sweden 2. Acreo Swedish ICT AB, Beta 2, Scheelev. 17, SE-223 70 Lund, Sweden

Nanowire, Doping, Hall effect, Electrical characterization

Electrical characterization of nanowires is a time-consuming and challenging task due to the complexity of single nanowire device fabrication and the difficulty in interpreting the measurements. We present a method to measure Hall effect in nanowires using a three-probe device that is simpler to fabricate than previous four-probe nanowire Hall devices and allows characterization of nanowires with smaller diameter. Extraction of charge carrier concentration from the three-probe measurements using an analytical model is discussed and compared to simulations. The validity of the method is experimentally verified by a comparison between results obtained with the three-probe method and results obtained using four-probe nanowire Hall measurements. In addition, a nanowire with a diameter of only 65 nm is characterized to demonstrate the capabilities of the method. The three-probe Hall effect method offers a relatively

fast and simple, yet accurate way to quantify the charge carrier concentration in nanowires and has the potential to become a standard characterization technique for nanowires.

Despite the rapid advance of semiconductor nanowire (NW) research in recent years, measuring the electrical properties and doping of NWs remains a challenging task. Many different measurement techniques, both electrical[1–8] and contact-less[9–16], have been demonstrated. However, few large-scale studies of doping of NWs have been published, likely due to the difficulties associated with interpretation of the data and the time-consuming device fabrication. The most widely used electrical method, field effect (FE) mobility measurements[1], is relatively simple in terms of device fabrication and measurements. However, the accuracy is often questioned and careful methodology is necessary in order to properly calculate the gate capacitance,[17–19] account for surface charge[20,21] and contact resistance[19,22]. Furthermore, due to the limited depletion width in a semiconductor, only thin NWs with relatively low doping concentration can be fully characterized in a FE mobility measurement.[19] In the last few years, it has also been demonstrated that Hall effect measurements can be used to characterize NWs.[5,6] This technique solves some of the problems with FE mobility measurements by directly probing the charge carrier concentration in the entire cross-section of the NW and not relying on an estimated gate capacitance. However, previous NW Hall devices have utilized a four-probe design (fig. 1a) with one Hall voltage probe on each side of the NW, a design resembling a traditional Hall bar structure. Fabrication of a device with such narrow and well-defined contact gap requires advanced processing with very high accuracy. The process becomes increasingly challenging as the NW diameter decreases, due to resolution limitations and the alignment accuracy of the electron beam lithography process used to define the contacts.

In this work, we present a method to carry out Hall effect characterization using a three-probe device geometry (fig. 1b). Instead of measuring the Hall voltage as the potential difference between two contacts on opposite sides of the NW, the Hall voltage is measured as the change in potential in a single contact as the strength of the applied magnetic field is varied. By using just one Hall contact, we circumvent the need for high resolution lithography and instead use a spacer layer to control the contact overlap. We discuss the extraction of charge carrier concentration from the measurements and validate the method experimentally by showing good correlation between results from three-probe Hall measurements and previous results obtained using four-probe NW Hall devices on NWs from the same growth series. Due to the relaxed requirements on alignment accuracy and resolution in the lithographic process, the three-probe method makes it possible to characterize NWs with smaller diameter than what has been possible previously. We show this by demonstrating Hall effect measurements on a NW with a diameter of only 65 nm.

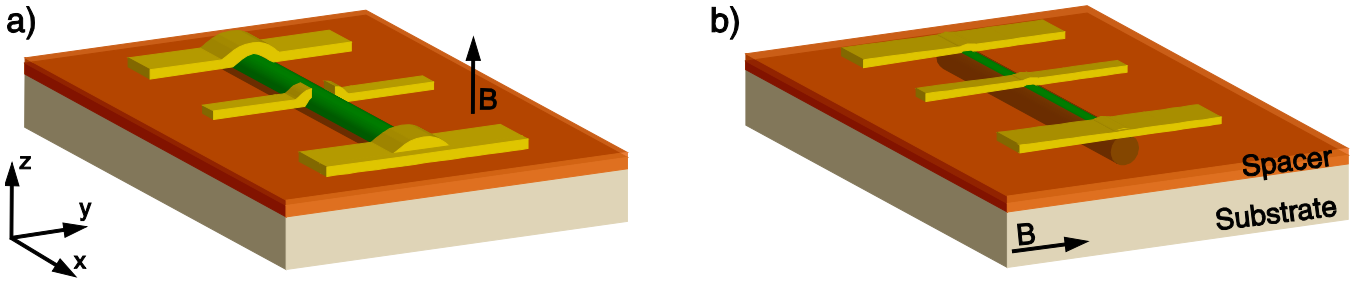

Figure 1. a) Four-probe NW Hall effect device. The current is fed in the x-direction, the magnetic field is applied in z and the Hall voltage is measured in the y-direction. b) Three-probe NW Hall effect device. The current is fed in the x-direction, the magnetic field is applied in y and the potential difference due to the Hall effect appears in z-direction.

As a test bed for this method, a series of S (H_2S) doped InP NWs grown with different dopant molar fractions (χ) were used. The NWs had diameters of approximately 200 nm and a length of 2.5 µm. The NWs were grown with highly doped ($\chi = 3.1 \cdot 10^{-5}$), 250 nm long segments at each end to facilitate ohmic contact formation. NWs from this growth series have previously been characterized with both Hall effect and FE measurements.[19] For more details on the NW growth, we refer to reference 19.

A cross-section schematic, an overview scanning electron microscopy image and a FIB cross-section of a device can be seen in figure 2. The devices were fabricated by first transferring NWs to a measurement substrate (Si, 100 nm SiO_2, 10 nm HfO_2) with predefined bond pads. Next, a polymer spacer layer (Shipley S1805:PGMA, 1:1) was spin coated on the sample at 3000 rpm for 60 s. The deposition parameters and ratio of the polymer mix was optimized to form a spacer with about the same thickness as the diameter of the NWs. The polymer layer was permanent baked at 200 °C for 10 minutes and then reactive ion etched (RIE) in O_2 plasma for 25 s in order clear the top facet of the NWs from resist. The polymer thickness and the RIE process controls how much of the NW perimeter will be contacted with metal. The central angle of the circular sector that is covered with metal will be referred to as the contact angle, α (fig. 2a). Contacts were then defined to the NWs using electron beam lithography (EBL) and metal (10 nm Ti followed by 100 nm Au) was deposited using thermal evaporation. This resulted in a lateral NW device with a contact angle of approximately 90°. Note that two separate Hall probes were defined at different positions along the NW, enabling two points of spatial resolution in the Hall measurement and also four-probe resistivity measurements.

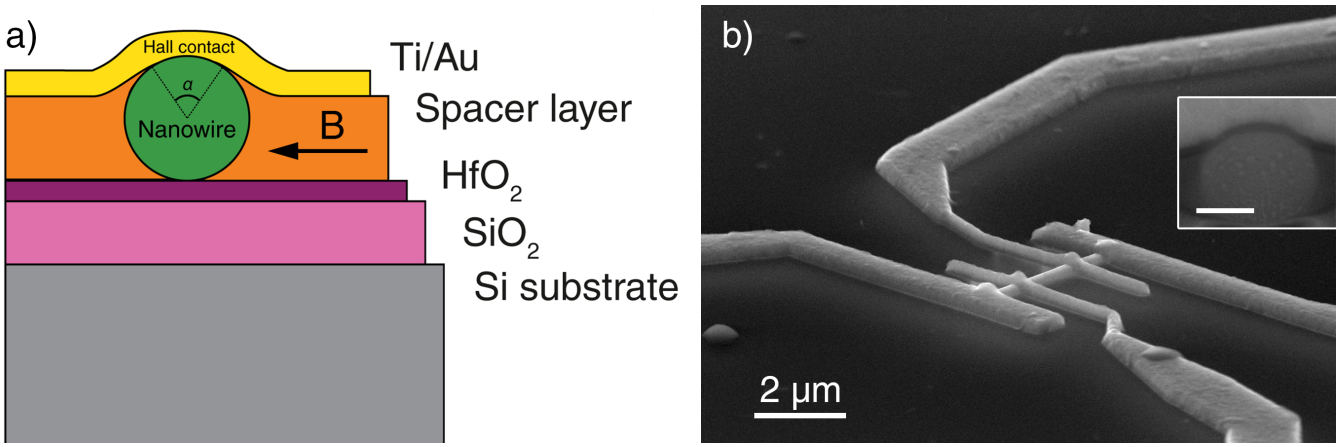

Figure 2. Three-probe NW Hall device. a) Schematic of the device in cross-section. The contact angle, α, is indicated. b) Scanning electron microscopy image of a device. Note that two Hall probes were used in this case, enabling two points of spatial resolution in the Hall measurement and four-probe resistivity measurements. Inset: FIB cross-section through contact and NW. Tilt angle 52°, scale bar 100 nm.

In a traditional four-probe Hall effect measurement, the Hall voltage is measured as the potential difference between two contacts on opposite sides of the sample, thereby canceling potential fluctuations that may occur if the resistance of the NW device fluctuates during the measurement. In the three-probe geometry, the Hall voltage is instead measured as the change in potential in a single contact (with respect to ground) as the strength of the applied magnetic field is varied. Since the potential is measured at a number of different magnetic fields sequentially, the measurement will be sensitive to drift in the NW potential, e.g. caused by fluctuations in the surface properties, charging effects or unstable contacts. It is therefore necessary to design the measurement so that drift effects can be separated from the actual Hall voltage. This was done by randomizing the order in which the magnetic fields were applied and by taking reference measurements at 0 T between each magnetic field (fig. 3a). To reveal magnetoresistance effects, the magnetic field sweep was centered around 0 T. The three-probe Hall voltage was then

extracted from the measurements as the difference between the measured potential at a certain magnetic field and the reference level, defined by a linear fit between the two surrounding 0 T reference measurements (fig. 3). The voltage was measured 300 times at each applied magnetic field. The current sourced through the NWs was 100 µA. All measurements were taken at room temperature.

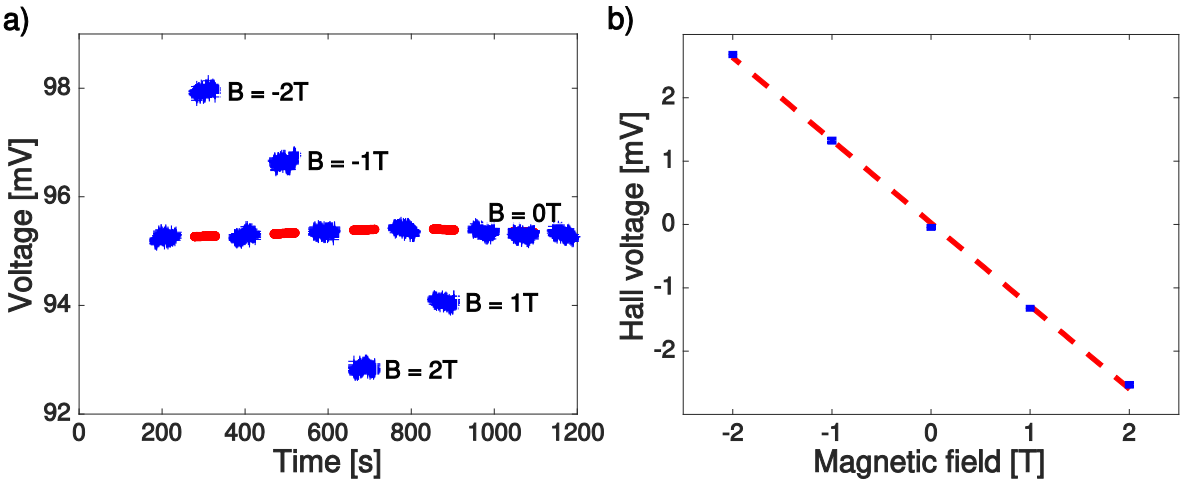

Figure 3. A representative three-probe NW Hall measurement. a) Measured potential in the Hall probe as function of time. Each cluster of data points contains 300 voltage measurements. The applied magnetic field is printed next to the data points. The red lines are linear fits between the closest 0 T reference measurements. b) Extracted Hall voltage as function of magnetic field. Here, the Hall voltage for each magnetic field is extracted as the difference between the reference level and the mean value of the 300 voltage measurements, with the errorbars showing the standard deviation. The dashed line is a linear fit to all the voltage measurements, before averaging.

Next, we discuss how to extract the carrier concentration from a three-probe Hall measurement. Again, the Hall voltage (V_H) is usually described as the voltage between the contacts on opposite sides of the sample. In a three probe measurement, only half of this voltage

is measured, since the change in potential is measured on just one side of the sample. The three probe Hall voltage is thus given by the equation

$V_{H,3p} = \frac{IB_y}{\pi nqr}$ (eq. 1),

where I is the current through the NW, B_y is the magnetic field, n is the charge carrier concentration, q is the carrier charge and r is the radius of the NW. Note that eq. 1 is simply the Hall voltage in a cylinder reduced by a factor of 2 and that this kind of analytic expression is valid only if the contacts can be considered point-like. In a real NW device this is rarely the case, and more careful analysis is necessary to investigate the validity of the model. To this end, a 3D finite element method (FEM) model implemented in COMSOL Multiphysics (R) was used. The potential and current in the NW was simulated by solving the current continuity equation and accounting for the Hall effect with an anisotropic conductivity tensor.[5] To simulate a non point-like metal contact, the Hall probe potential was defined as the electric potential in an iso-potential area on a metal layer. The boundary condition of the iso-potential was that the integrated current density over the contact area is zero, allowing current to enter the contact at one point and leave it somewhere else. Contact resistivity (ρ_c), was defined as a resistive boundary at the metal/semiconductor interface. In the simulations, the electrical dimensions were assumed to be equal to the physical dimensions and the carrier mobility was fixed to 1000 $cm^2/(Vs)$, based on experimental data from previous measurements. The fixed mobility does not affect the magnitude of the Hall voltage developed in the NW. It does have an effect on the magnitude of current shunting through the contacts, but for reasonable mobility values the difference is negligible. It is important to note that if the NW radius is comparable to the carrier screening length, i.e. in thin NWs with low doping level, diffusion currents will counteract the charge build-up and limit the Hall voltage.[23] The model used in this work only considers drift

current and is thus only valid when the NW radius is considerably larger than the screening length, which is the case for the doping levels and NW radii considered in the simulations presented here. Using the method from reference 23, the reduction in Hall voltage due to diffusion currents was calculated to be less than 10% for all the simulated devices.

Two main mechanisms can be identified to cause deviation from the ideal case described by the analytic expression (eq. 1), both stemming from shunting effects of the metal contacts. First, by placing metal contacts on the NW, the contact forms a potential iso-surface on the NW and the Hall voltage cannot be considered to be probed only in a single point at the top where it is the largest. The Hall voltage is thus shunted in the vertical direction (z-direction in fig. 1b). The second deviation is due to the formation of an alternative longitudinal (x-direction in fig. 1b) current path when a metal contact is placed on the NW. When current is shunted through the metal, the current density in the NW underneath the contact is reduced, causing a decrease in the Hall voltage.

The effects of voltage shunting in the vertical direction and current shunting in the longitudinal direction are vital in understanding the simulation results presented in fig. 4 (normalized with eq. 1). First (fig. 4a), we examine the effect of contact angle for the case when the contact resistivity is relatively large ($\rho_c = 10^{-5}$ Ωcm^2). Here the current shunting effect is small due to the large resistance of the shunt path. Instead, voltage shunting in the vertical direction is the main reason for the increasing deviation from eq. 1 (i.e. normalized Hall voltage deviating from 1) as the contact angle (α) is increased. The Hall voltage deviates only slightly from eq. 1 for small contact angles and it is also interesting to note that Hall voltage can be observed even when $\alpha = 180°$, meaning that the spacer layer may not be strictly necessary if the contact is deposited from the top, e.g. by thermal evaporation. The voltage shunting is further illustrated in the supporting

information (fig. S1), where the potential distribution in the center cross-section of a device with contact angle 180° is shown.

Second, we examine the effect of contact resistivity (ρ_c) on the Hall voltage. In fig. 4b, the normalized Hall voltages for different contact angles are shown as function of ρ_c. It can be seen that the Hall voltage decreases when the contact resistivity becomes smaller, which can be explained by the decreasing resistance of the shunt path causing more current to be shunted through the metal contact. A device with a contact width (w_c) of only 50 nm (compared to 100 nm for the other simulated devices) is also included in fig. 4b. Since the low resistance metallic shunt path is shorter in this device, the effect of current shunting is correspondingly less pronounced. It would therefore be desirable to design the Hall devices with very narrow contacts, however this is associated with fabrication challenges.

Third (fig. 4c), we investigate the effect of the NW carrier concentration on the normalized Hall voltage. It can be seen that the dependence of contact resistance is more pronounced for lower carrier concentrations, since the current shunting effect is not only dependent on the contact resistance, but rather on the ratio between the resistance of the NW and the resistance of the shunt path.

Finally, we observe that the reduction of Hall voltage due to current shunting is larger for NWs with small radii (fig. 4d) because of the increase in NW resistance and the on average shorter vertical distance to the contact, giving a lower average resistance for the current to reach the shunt path. This, in combination with the diffusion current effect, may be limiting factors for how small NWs can be characterized using Hall effect measurements.

It should be noted that the shunting effects are not only present in three-probe NW Hall devices, but also in four-probe devices. The effect was discussed by Barbut et al.[24], but without

consideration of the resistance at the semiconductor-metal interface. It is also interesting to note that in some cases magnetoresistance effects could be observed in the simulations. If the resistance in the NW increases when a magnetic field is applied, the potential in the voltage probe increases (assuming a constant current). Since this magnetoresistance effect is symmetric around 0 T, the effect manifests as a curvature in the Hall voltage with respect to magnetic field. This effect was only observed in simulations of short devices with very high mobility, and the experimental data showed no such effects.

To summarize the simulation results, we see that to characterize a NW with Hall effect measurements, it is desirable to keep the contact angle small and the resistance of the shunt path high compared to the NW resistance. It should be noted that for most III-V materials it is very challenging to reach contact resistivities on the low end of the range simulated here.[25] The simulations presented in fig. 4 can be used as a guide for device design and provide correction factors for eq. 1 when extracting charge carrier concentration from measurements. For the devices measured in this work, the contact resistance was high enough ($> 10^{-7}$ Ωcm^2) that the current shunting effect could be deemed negligible. Therefore, to extract the carrier concentrations presented next, the only correction made to eq. 1 was for voltage shunting caused by the 90° contact angle in our devices (fig. 4a).

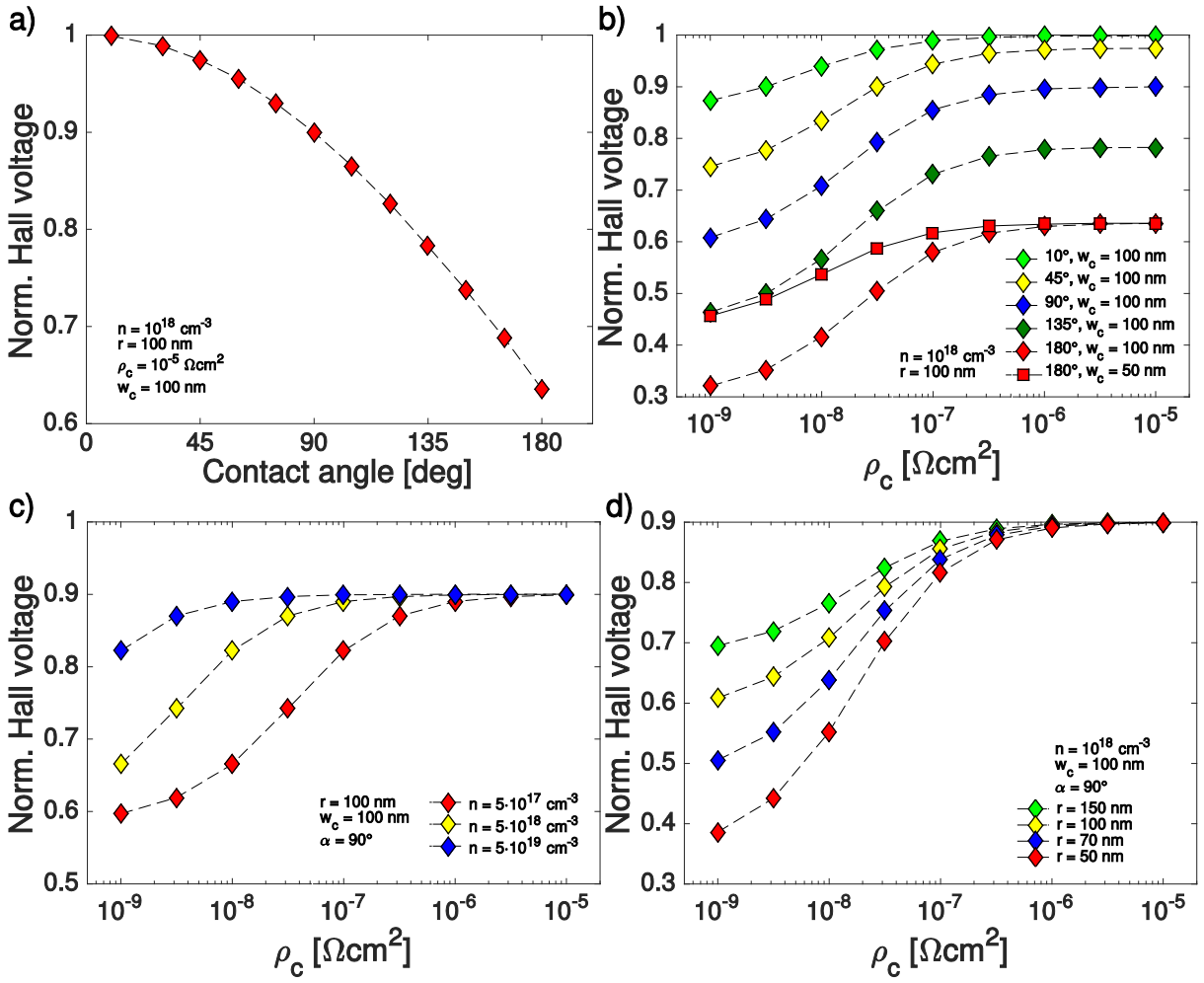

Figure 4. Simulated reduction of Hall voltage in three-probe NW Hall devices caused by non-point-like contacts. The simulated Hall voltage, normalized with eq. 1, is plotted: a) as function of contact angle for a device with large contact resistance. Vertical voltage shunting is the dominating effect and the Hall voltage deviates only slightly from eq. 1 for small contact angles. b) for different contact angles, plotted as function of contact resistivity. The current shunting increases with decreasing contact resistivity and severely affects the Hall voltage for $\rho_c < 10^{-7}\ \Omega\text{cm}^2$. For the device with $w_c = 50$ nm, the shunting effect is reduced. c) for different charge carrier concentrations. The current shunting effect is larger for lower carrier concentrations due to the larger ratio between the resistance of the NW and the resistance of the

shunt path. d) for different NW radii. The shunting effect is more prominent for smaller NW radii.

Figure 5 shows the measured charge carrier concentrations as function of the dopant molar fraction during growth for both four-probe NW Hall effect measurements (as presented previously in ref [19]) and three-probe Hall effect measurements. The correlation is good, giving experimental evidence that the charge carrier concentration can be accurately measured in the three-probe Hall geometry. No clear spatial dependence was found for the measured carrier concentrations, so all measured values are treated as individual data points. The diameters of the investigated nanowires range from 190-240 nm. The measured Hall mobility is presented in the supporting information (fig. S2).

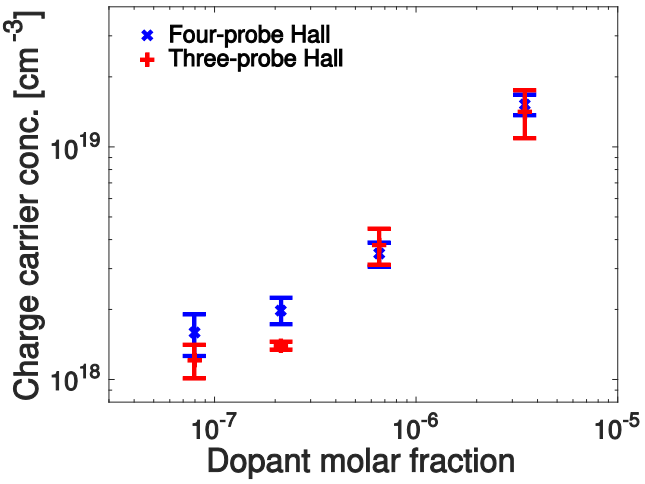

Figure 5. Comparison of measured charge carrier concentration between four-probe NW Hall effect measurements and three-probe NW Hall effect measurements. The data points show the average charge carrier concentration of the measured devices as function of the dopant gas molar fraction at growth, with the errorbars showing the standard deviation of the measured values. The total number of measured carrier concentrations was 28 for four-probe Hall and 21 for three-probe Hall.

The main drawback of the three-probe method compared to four-probe Hall measurements, is the previously discussed sensitivity to drift in the NW potential. It is necessary to design the experiment so that a drift in potential cannot be misinterpreted as a Hall voltage and it should be noted that for devices more prone to drift, more sophisticated drift correction methods than the ones used in this work could be necessary. For high accuracy, it is also important to design the devices as to minimize the shunting effects, i.e. to make the contacts as point-like as possible. Even though this can be accounted for in a simulation, it adds an uncertainty to the quantification.

A significant advantage of the three-probe Hall method, compared to four-probe NW Hall effect measurements, is that it removes the lithographic constraints on the NW diameters accessible for characterization. Previously, NW Hall devices have been demonstrated by DeGrave et al.[26] with a NW (Si) diameter of 100 nm and by Storm et al.[5] with a NW (InP) diameter of 80 nm. However, no measurement data was presented for these devices. In fig. 6a we present a three-probe Hall device with a 65 nm diameter NW (Sn doped InP, growth details in supporting information). Hall effect measurements on the device (fig. 6b) and charge carrier concentration extraction using a correction factor from fig. 4a ($\alpha = 120°$, $\rho_c > 10^{-7}$ Ωcm^2) determined the charge carrier density to $2 \cdot 10^{18}$ cm^{-3}. If the diffusion current reduction presented in ref 23 is considered, this value is reduced by 10%. This measurement shows the potential of the three-probe Hall method to characterize thinner NWs than what has been possible previously with post-processed four-probe Hall contacts.

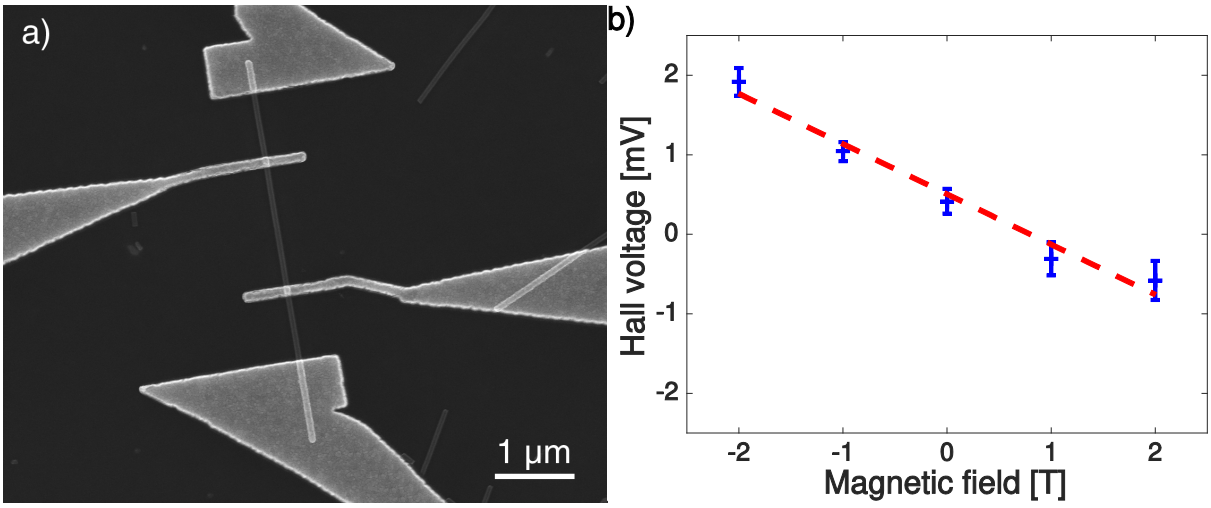

Figure 6. Hall effect characterization of a NW with a diameter of only 65 nm. a) Top view scanning electron microscopy image of the device. b) Hall voltage as function of magnetic field. Each data point is an average of 200 voltage measurements, with the errorbars showing the standard deviation. The dashed line is a linear fit to the data.

We note that although the carrier concentration could be measured successfully, conducting measurements on thinner NWs proved more challenging than on the thicker NWs. The measured carrier concentrations were more scattered and there was significantly more drift in the measurements. In addition to fabrication challenges and the shunting effects discussed previously, there are also other factors making Hall effect measurements on thinner NWs more challenging. A thinner NW is more susceptible to external perturbations such as surface charges, environment and influence from the contacts. E.g. a Schottky contact deposited on a low doped NW can significantly alter the potential structure and charge carrier concentration locally. The Hall voltage in thin NWs with low doping levels will also be limited by diffusion currents. It is certainly possible to account for these effects through simulations, although it requires experimental data that are not always easily attainable. The topic warrants further investigation.

In summary, we present a simple three-probe device to measure Hall effect in NWs. The device design significantly relaxes the requirements on nanofabrication precision compared to previous four-probe NW Hall devices and allows characterization of thinner NWs. We discuss extraction of charge carrier concentration data from the measurements and show good correlation between the three-probe method and previous four-probe NW Hall measurements on NWs from the same growth series. The three-probe Hall method offers a relatively fast and simple, yet accurate way to quantify the charge carrier concentration in NWs and has the potential to become a standard characterization technique for nanowires.

ASSOCIATED CONTENT

Supporting Information.

Simulated electric potential in Hall device cross-section (Fig. S1). Measured Hall mobility (Fig. S2). Details on nanowire growth. This material is available free of charge via the Internet at http://pubs.acs.org.

AUTHOR INFORMATION

Corresponding Author

* lars.samuelson@ftf.lth.se

Author Contributions

O.H. designed the experiment and devices, did sample fabrication, measurements, data analysis and wrote the paper. G.O. grew the nanowires, helped write the paper and participated in

discussions. L.S. participated in discussions and supervised the project. K.S. participated in the discussions and supervised the project. All authors reviewed the manuscript.

ACKNOWLEDGMENT

This work was carried out within Lund Nano Lab and was supported by NanoLund, Swedish Foundation for Strategic Research (SSF) (EM11-0015), Swedish Energy Agency (Energimyndigheten) (2012-004607), Knut and Alice Wallenberg foundation (KAW) (2013.0284), the Swedish Research Council (VR) (621-2012-4185) and EU Horizon 2020 grant agreement No 641023 (Nano-Tandem). This publication reflects only the author's views and the funding agency is not responsible for any use that may be made of the information it contains.

REFERENCES

(1) Cui, Y.; Duan, X.; Hu, J.; Lieber, C. M. Doping and Electrical Transport in Silicon Nanowires. *J. Phys. Chem. B* **2000**, *104*, 5213–5216.

(2) Roddaro, S.; Nilsson, K.; Astromskas, G.; Samuelson, L.; Wernersson, L. E.; Karlström, O.; Wacker, A. InAs Nanowire Metal-Oxide-Semiconductor Capacitors. *Appl. Phys. Lett.* **2008**, *92*, 253509.

(3) Garnett, E. C.; Tseng, Y.-C.; Khanal, D. R.; Wu, J.; Bokor, J.; Yang, P. Dopant Profiling and Surface Analysis of Silicon Nanowires Using Capacitance-Voltage Measurements. *Nat. Nanotechnol.* **2009**, *4*, 311–314.

(4) Mansfield, L. M.; Bertness, K. A.; Blanchard, P. T.; Harvey, T. E.; Sanders, A. W.; Sanford, N. A. GaN Nanowire Carrier Concentration Calculated from Light and Dark Resistance Measurements. *J. Electron. Mater.* **2009**, *38*, 495–504.

(5) Storm, K.; Halvardsson, F.; Heurlin, M.; Lindgren, D.; Gustafsson, A.; Wu, P. M.; Monemar, B.; Samuelson, L. Spatially Resolved Hall Effect Measurement in a Single Semiconductor Nanowire. *Nat. Nanotechnol.* **2012**, *7*, 718–722.

(6) Blömers, C.; Grap, T.; Lepsa, M. I.; Moers, J.; Trellenkamp, S.; Grützmacher, D.; Lüth, H.; Schäpers, T. Hall Effect Measurements on InAs Nanowires. *Appl. Phys. Lett.* **2012**, *101*, 152106.

(7) Tchoulfian, P.; Donatini, F.; Levy, F.; Amstatt, B.; Dussaigne, A.; Ferret, P.; Bustarret, E.; Pernot, J. Thermoelectric and Micro-Raman Measurements of Carrier Density and Mobility in Heavily Si-Doped GaN Wires. *Appl. Phys. Lett.* **2013**, *103*, 202101.

(8) Schmidt, V.; Mensch, P. F. J.; Karg, S. F.; Gotsmann, B.; Das Kanungo, P.; Schmid, H.; Riel, H. Using the Seebeck Coefficient to Determine Charge Carrier Concentration, Mobility, and Relaxation Time in InAs Nanowires. *Appl. Phys. Lett.* **2014**, *104*, 12113.

(9) Perea, D. E.; Allen, J. E.; May, S. J.; Wessels, B. W.; Seidman, D. N.; Lauhon, L. J. Three-Dimensional Nanoscale Composition Mapping of Semiconductor Nanowires. *Nano Lett.* **2006**, *6*, 181–185.

(10) Stoica, T.; Meijers, R. J.; Calarco, R.; Richter, T.; Sutler, E.; Lüth, H. Photoluminescence and Intrinsic Properties of MBE-Grown InN Nanowires. *Nano Lett.* **2006**, *6*, 1541–1547.

(11) Huber, A. J.; Keilmann, F.; Wittborn, J.; Aizpurua, J.; Hillenbrand, R. Terahertz Near-Field Nanoscopy of Nanodevices. *Nano Lett.* **2008**, *8*, 3766–3770.

(12) Parkinson, P.; Joyce, H. J.; Gao, Q.; Tan, H. H.; Zhang, X.; Zou, J.; Jagadish, C.; Herz, L. M.; Johnston, M. B. Carrier Lifetime and Mobility Enhancement in Nearly Defect-Free

Core- Shell Nanowires Measured Using Time-Resolved Terahertz Spectroscopy. *Nano Lett.* **2009**, *9*, 3349–3353.

(13) Stiegler, J. M.; Huber, A. J.; Diedenhofen, S. L.; Gómez Rivas, J.; Algra, R. E.; Bakkers, E. P. A. M.; Hillenbrand, R. Nanoscale Free-Carrier Profiling of Individual Semiconductor Nanowires by Infrared near-Field Nanoscopy. *Nano Lett.* **2010**, *10*, 1387–1392.

(14) Ketterer, B.; Uccelli, E.; Fontcuberta i Morral, A. Mobility and Carrier Density in P-Type GaAs Nanowires Measured by Transmission Raman Spectroscopy. *Nanoscale* **2012**, *4*, 1789–1793.

(15) Seo, M. A.; Yoo, J.; Dayeh, S. A.; Picraux, S. T.; Taylor, A. J.; Prasankumar, R. P. Mapping Carrier Diffusion in Single Silicon Core-Shell Nanowires with Ultrafast Optical Microscopy. *Nano Lett.* **2012**, *12*, 6334–6338.

(16) Lindgren, D.; Hultin, O.; Heurlin, M.; Storm, K.; Borgström, M. T.; Samuelson, L.; Gustafsson, A. Study of Carrier Concentration in Single InP Nanowires by Luminescence and Hall Measurements. *Nanotechnology* **2015**, *26*, 45705.

(17) Wunnicke, O. Gate Capacitance of Back-Gated Nanowire Field-Effect Transistors. *Appl. Phys. Lett.* **2006**, *89*, 83102.

(18) Khanal, D. R.; Wu, J. Gate Coupling and Charge Distribution in Nanowire Field Effect Transistors. *Nano Lett.* **2007**, *7*, 2778–2783.

(19) Hultin, O.; Otnes, G.; Borgström, M. T.; Björk, M.; Samuelson, L.; Storm, K. Comparing Hall Effect and Field Effect Measurements on the Same Single Nanowire. *Nano Lett.*

2016, *16*, 205–211.

(20) Khanal, D. R.; Walukiewicz, W.; Grandal, J.; Calleja, E.; Wu, J. Determining Surface Fermi Level Pinning Position of InN Nanowires Using Electrolyte Gating. *Appl. Phys. Lett.* **2009**, *95*, 173114.

(21) Heedt, S.; Otto, I.; Sladek, K.; Hardtdegen, H.; Schubert, J.; Demarina, N.; Lüth, H.; Gruetzmacher, D.; Schäpers, T. Resolving Ambiguities in Nanowire Field-Effect Transistor Characterization. *Nanoscale* **2015**, *7*, 18188–18197.

(22) Gül, Ö.; Woerkom, D. J. Van; Weperen, I. Van; Car, D.; Plissard, S. R.; Bakkers, E. P. A. M.; Kouwenhoven, L. P. Towards High Mobility InSb Nanowire Devices. *Nanotechnology* **2015**, *26*, 215202.

(23) Fernandes, C.; Ruda, H. E.; Shik, A. Hall Effect in Nanowires. *J. Appl. Phys.* **2014**, *115*, 234304.

(24) Barbut, L.; Jazaeri, F.; Bouvet, D.; Sallese, J. Mobility Measurement in Nanowires Based on Magnetic Field-Induced Current Splitting Method in H-Shape Devices. *IEEE Trans. Electron Devices* **2014**, *61*, 2486–2494.

(25) Baca, A. G.; Ren, F.; Zolper, J. C.; Briggs, R. D.; Pearton, S. J. A Survey of Ohmic Contacts to III-V Compound Semiconductors. *Thin Solid Films* **1997**, *308–309*, 599–606.

(26) DeGrave, J. P.; Liang, D.; Jin, S. A General Method to Measure the Hall Effect in Nanowires: Examples of FeS2 and MnSi (Supporting information). *Nano Lett.* **2013**, *13*, 2704–2709.

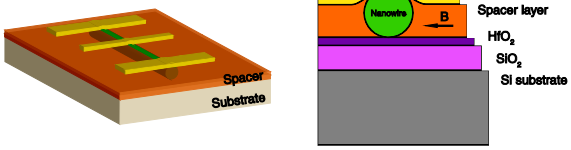
Spacer
Substrate

Nanowire
B
Ti/Au
Spacer layer
HfO2
SiO2
Si substrate